J|A|C|S
A R T I C L E S

Specific Ethene Surface Activation on Silver Oxide Covered Ag{111} from the Interplay of STM Experiment and Theory

Marie-Laure Bocquet, Philippe Sautet, Jorge Cerda,[†] Christopher I. Carlisle,[‡]
Matthew J. Webb,[‡] and David A. King*,[‡]

*Contribution from the Institut de Recherches sur la Catalyse, CNRS, 2 av. A. Einstein,
69626 Villeurbanne Cedex and Laboratoire de Chimie Théorique et des Matériaux hybrides,
Ecole Normale Supérieure, Lyon, France, Department of Chemistry, University of Cambridge,
Lensfield Road, Cambridge, CB2 1EW, U.K., and Instituto de Ciencia de Materiales de Madrid,
CSIC, Cantoblanco, 28049 Madrid, Spain*

Received July 10, 2002 ; E-mail: dak10@cus.cam.ac.uk

Abstract: High-resolution scanning tunneling microscopy (STM) images at 5 K, simultaneously resolving the molecular adsorbate and the honeycomb structure of the well-defined Ag{111}-p(4 × 4)+Ag$_{1.83}$O substrate, assign the adsorption site for ethene on the silver oxide surface. Ethene molecules are exclusively adsorbed above a particular subset of Ag$^{\delta+}$ sites in the hexagonal rings of the oxide. Extensive density functional theory (DFT) slab calculations confirm that this is the most stable site, with an adsorption energy of 0.4 eV (39 kJ mol^{-1}). Adsorption is accompanied by a large deformation of the hexagonal oxide ring and a significant increase in the C−C bond length. STM image simulations provide qualitative agreement with the experimental images, and the molecular orientation is discussed with the help of simple molecular orbital arguments.

Introduction

The oxygen-promoted reconstruction of the Ag{111} surface is of direct significance to an important industrial catalytic process, the partial oxidation of ethene to ethene epoxide, C_2H_4O. Despite numerous studies,[1] a full description of this reaction is still lacking. The present paper is one of a series in which we have systematically attempted to provide a basis for an atomic scale description of this reaction, using scanning tunneling microscopy at 5 K, STM simulations, and density functional theory slab calculations.[2−4]

Atomic imaging studies of oxygen on Ag{111} revealed just two distinct adsorbate phases.[3] At coverages ≤0.05 monolayers (ML), individual oxygen adatoms are randomly adsorbed, with a large near-neighbor exclusion zone. At higher coverage, regular islands of a p(4 × 4)-O phase are nucleated, which eventually cover the whole surface at annealing temperatures of ∼470 K. The structure of the oxide phase has been determined by STM imaging and simulations[2] and by DFT slab calculations.[4] It is composed of hexagonal O−Ag−O rings of 6.7 Å diameter and Ag atoms on threefold hollow sites of the Ag{111} surface at the ring centers. These are the only adatoms

resolved in the experimental images. Compared with a Ag$_2$O layer, Ag adatoms on atop sites are missing, which accounts for the Ag$_{1.83}$O stoichiometry. The stability of the oxide phase has been theoretically determined over a wide range of temperatures and pressures.[4] Under ultrahigh vacuum conditions, the oxide, which is the most stable phase at low temperatures, yields to the low-coverage O adatom phase at 470 K, in close agreement with experiment.[3] At oxygen pressures and temperatures consistent with real catalytic partial oxidation conditions, P_{O2}=15 bar, T = 550 K,[5] these DFT-based free-energy calculations predict that the Ag$_{1.83}$O film is the most stable phase on Ag{111}.[4] This is apparently, therefore, the template for the partial oxidation of ethene.

The interaction of oxygen with silver surfaces has also been studied using clusters, both to study oxygen adsorption[6] and epoxidation.[7] Here we note that, while gradient-density corrected DFT slab calculations which have been fully converged show remarkably good quantitative agreement with experimentally determined structures and good agreement with experimental calorimetric adsorption energies,[8] cluster calculations do not match up to experiment in the same way. In parallel with our work, DFT slab calculations have been performed by Li et al.[9] using unit cells with oxygen, corresponding to coverages at and above 0.25 ML.

† Instituto de Ciencia de Materiales de Madrid.
‡ University of Cambridge.
(1) Vansanten, R. A.; Kuipers, H. *Adv. Catal.* **1987**, *35*, 265−321.
(2) Carlisle, C. I.; King, D. A.; Bocquet, M. L.; Cerda, J.; Sautet, P. *Phys. Rev. Lett.* **2000**, *84*, 3899−3902.
(3) Carlisle, C. I.; Fujimoto, T.; Sim, W. S.; King, D. A. *Surf. Sci.* **2000**, *470*, 15−31.
(4) Michaelides, A.; Bocquet, M. L.; Sautet, P.; Alavi, A.; King, D. A. *Chem. Phys. Lett.* **2003**, *367*, 344−350.

(5) Berty, J. M. *Appl. Ind. Catal.* **1983**, *1*.
(6) Saravanan, C.; Salazar, M. R.; Kress, J. D.; Redondo, A. *J. Phys. Chem. B* **2000**, *104*, 8685−8691.
(7) Avdeev, V. I.; Zhidomirov, G. M. *Surf. Sci.* **2001**, *492*, 137−151.
(8) Ge, Q. F.; Kose, R.; King, D. A. *Adv. Catal.* **2000**, *45*, 207−259.
(9) Li, W. X.; Stampfl, C.; Scheffler, M. *Phys. Rev. B* **2002**, *65*, art. no.-075407.

While it is generally accepted that atomic oxygen (O_a) leads to the total combustion of ethene, some controversy exists as to the nature of the epoxidizing oxygen species. Studies by Grant and Lambert[10] showed that for both epoxidation and total combustion, the yield of adsorbed dioxygen (O_{2a}) from the substrate remained unchanged, while a marked attenuation of the desorption peaks related to O_a was observed. This was supported experimentally by van Santen and de Groot, providing additional evidence for partial oxidation in the absence of O_2.[11] A complication appears to be that the O_a species is capable of reacting in two different ways, with the selectivity being altered by the reaction conditions and in particular by the addition of promoters. As a result, several authors have indicated the importance of subsurface O_a in the promotion of the partial oxidation reaction.[12,13] Chemisorbed dioxygen was proposed as the active species in the work of Kilty and Sachtler[14] and later by the work of Campbell.[15−20] Specifically, epoxidation rates were observed to be similar on Ag{110} and Ag{111}, despite the rate of dissociation of dioxygen being a factor of ∼50 slower on the latter. Recent theoretical studies, based primarily on cluster calculations, additionally support dioxygen epoxidation.[21,22]

In this paper, we provide new insights into the mechanism of catalytic epoxidation by considering the adsorption of ethene on the p(4 × 4)+Ag$_{1.83}$O superstructure described above. STM images resolving both the molecule and the underlying oxide after ethene deposition on this phase are presented and discussed. On the basis of these images, extensive DFT calculations have been performed to determine the orientation and geometry of the adsorbed ethene with respect to the oxide rings. In addition, STM simulations have been carried out for the optimized structure, yielding good agreement with experiment. Finally, the electronic origin of the preferred adsorption geometry is rationalized by considering the atomically projected density of states (DOS).

Experimental Methods

Experiments were carried out in an ultrahigh vacuum (UHV) system housing a low-temperature STM (Omicron) maintained at a base pressure of 1×10^{-10} mbar, previously described in detail.[3] The STM head is attached to the base of a cylindrical bath cryostat containing liquid helium, liquid nitrogen, or air for operation at crystal temperatures of 5, 77, and 298 K, respectively. The Ag crystal, cut to within 0.5° of the {111} plane, was prepared by repeated cycles of ion sputtering and annealing. Argon sputtering was conducted at a sample temperature of 600 K, followed by sample annealing at 780 K. Prior to dosing, the LEED pattern showed a sharp (1 × 1) structure for the clean surface; no significant impurities were seen with Auger analysis and the STM showed large, clean, and relatively defect-free terraces. The preparation of the p(4 × 4)+Ag$_{1.83}$O reconstructed surface has been described in detail elsewhere.[2] Because of the low dissociative sticking probability of O_2 on Ag{111}, NO$_2$ was used as the source of oxygen following

(10) Grant, R. B.; Lambert, R. M. *J. Catal.* **1985**, *92*, 364−375.
(11) Vansanten, R. A.; Degroot, C. P. M. *J. Catal.* **1986**, *98*, 530−539.
(12) Vandenhoek, P. J.; Baerends, E. J.; Vansanten, R. A. *J. Phys. Chem.* **1989**, *93*, 6469−6475.
(13) Tan, S. A.; Grant, R. B.; Lambert, R. M. *J. Catal.* **1987**, *104*, 156−163.
(14) Kilty, P. A.; Sachtler, W. H. H. *Catal. Rev. Sci. Eng.* **1974**, *10*.
(15) Campbell, C. T. *J. Phys. Chem.* **1985**, *89*, 5789−5795.
(16) Campbell, C. T. *ACS Symposium Series* **1985**, *288*, 210−221.
(17) Campbell, C. T. *J. Catal.* **1985**, *94*, 436−444.
(18) Campbell, C. T.; Koel, B. E. *J. Catal.* **1985**, *92*, 272−283.
(19) Campbell, C. T.; Paffett, M. T. *Appl. Surf. Sci.* **1984**, *19*, 28−42.
(20) Campbell, C. T. *J. Vac. Sci. Technol., A* **1984**, *2*, 1024−1027.
(21) Salazar, M. R.; Kress, J. D.; Redondo, A. *Catal. Lett.* **2000**, *64*, 107−111.
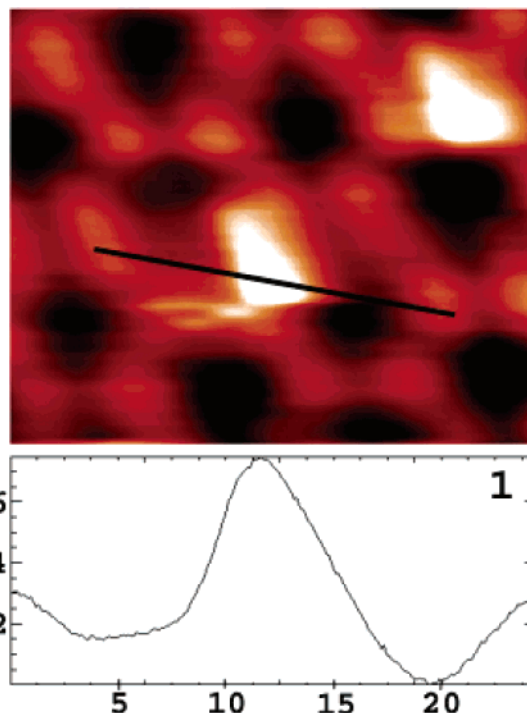(22) Nakatsuji, H.; Nakai, H.; Ikeda, K.; Yamamoto, Y. *Surf. Sci.* **1997**, *384*, 315−333.

Figure 1. High-resolution experimental STM topographic image of ethene adsorbates on the p(4 × 4)+Ag$_{1.83}$O structure at low coverage. A depth profile is shown for the corresponding line over the adsorption site, above a Ag$_3$ site in the oxide layer directly between the resolved Ag$_{1−2}$ atoms of the reconstruction (image conditions: 30 Å × 30 Å, 5 K, 0.061 V, 1.076 nA).

the procedure of Bare et al.[23] The crystal was exposed to a 600 L dose of NO$_2$ at a sample temperature of 480 K, producing a sharp (4 × 4) LEED pattern indicating oxide formation. The surface was then exposed to a low dose of ethene at 77 K, subsequently cooled to 5 K, and imaged using an etched tungsten tip.

Experimental Results and Discussion

Low-Coverage Regime. A high-resolution image of two ethene molecules adsorbed on the p(4 × 4)+Ag$_{1.83}$O structure following a low-exposure dose at 77 K is shown in Figure 1. Each bright spot is a single ethene molecule adsorbed on the characteristic honeycomb structure of the oxide, which is resolved in the background. The structure of the silver oxide film is shown schematically in Figure 2, and the caption defines the various Ag atoms and ions in the structure, following the previous definitions.[2] Close inspection of Figure 1 provides a determination of the adsorption site for ethene on the reconstructed surface as being directly between two bright features of the hexagonal pattern of the oxide, attributed to metallic Ag adatoms (Ag$_{1−2}$), and centered above a Ag$^{\delta+}$ site (Ag$_3$). The molecular protrusion is 0.5−1.0 Å higher than the honeycomb oxide and shows pronounced elongation perpendicular to the hexagon perimeter of the oxide ring. The Ag ionic site is common to all ethene molecules observed on the p(4 × 4)-Ag$_{1.83}$O structure.

High-Coverage Regime. By increasing the ethene exposure, further adsorption on the oxide structure is exclusively observed on the same sites as identified at low coverage, producing a saturated overlayer with all electrophilic Ag$_3$ sites occupied. It is significant that no further adsorption of ethene is observed

(23) Bare, S. R.; Griffiths, K.; Lennard, W. N.; Tang, H. T. *Surf. Sci.* **1995**, *342*, 185−198.
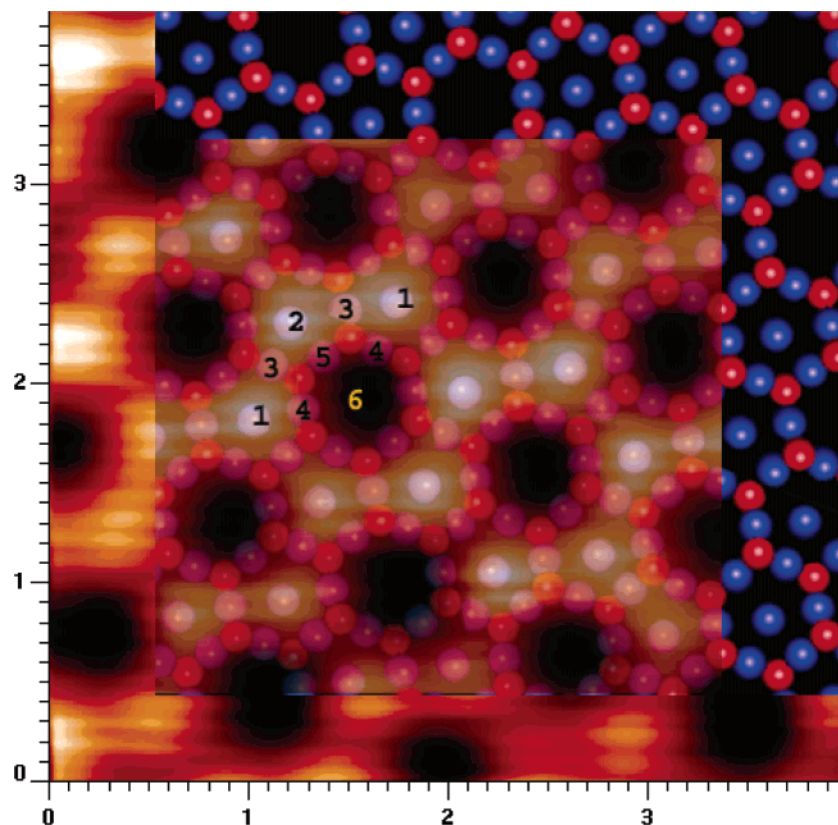
Figure 2. Montage image combining an STM image of the oxide structure (from bottom left) superimposed over the proposed oxide structure (from top right). The numbers shown, $n = 1-5$, correspond to the symmetrically different silver positions Ag_n within the middle silver layer sandwiched between the O_u and O_d layers. In electronic terms, Ag_1 and Ag_2 have metallic character, as they are exclusively bonded to silver atoms in the substrate below, whereas Ag_3, Ag_4, and Ag_5 are directly bonded to oxygen inside the oxide rings and are electrophilic (or ionic) in nature. Both Ag_4 and Ag_5 sites sit above threefold sites of the underlying {111} lattice atoms, whereas the Ag_3 occupies an atop site. This difference in coordination induces a buckling within the layer, determined in previous study to be 0.4 Å.[4]

after all these sites are occupied. At saturation, the ratio of $O:C_2H_4$ is 2:1; this saturation coverage may be simply attributable to a strong preference for the $Ag^{\delta+}$ sites discussed in detail below. A large area scan is shown in Figure 3 demonstrating decoration of all these sites; the inset shows that adsorption at each individual Ag_3 site can be resolved. At this coverage, the size of each protrusion is smaller than for the low-coverage adsorbate image. This may be attributed to intermolecular interactions hindering adsorbate motion around the site making the molecule more stable under the action of the scanning tip. In effect, ethene adsorption to saturation results in decoration of all Ag_3 sites, producing bright spots at these sites which are not otherwise imaged by the STM.[2,3]

Although the same ethene site on the oxide is assigned at high and low coverage, it is not possible to directly determine the molecular orientation; the adsorbates show no internal structure in the STM images. Increasing the temperature results in the onset of diffusion of ethene over the oxide structure. Images obtained at 77 K do not demonstrate adsorbate resolution, but instead we observe a streaky appearance across the bright features of the oxide lattice indicating the presence of mobile adsorbates with site occupation times that are much shorter than the scan rate at 77 K.

Theoretical Calculations

A first-principles density functional theory approach with the VASP (Vienna Ab initio Simulation Program)[24-26] code was
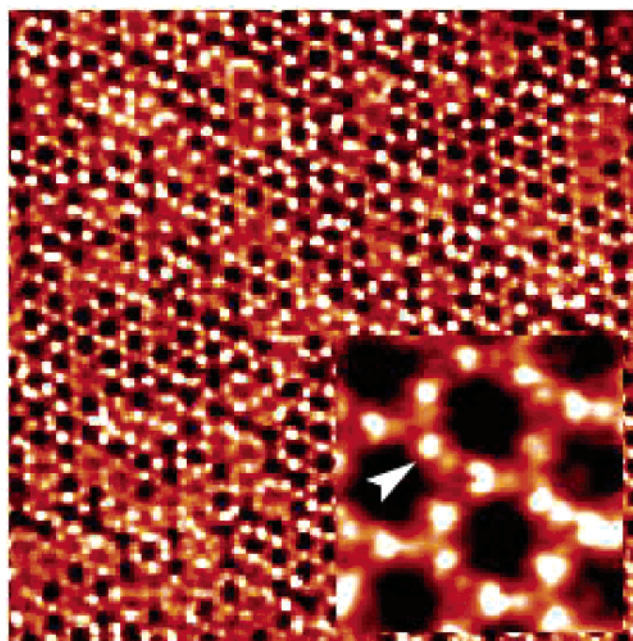

Figure 3. Experimental STM image of the high-coverage regime; the large area image shows saturation of all Ag_3 sites (image conditions: 280 Å × 280 Å, 77 K, 0.028 V, 0.131 nA); inset is a topographic image detailing the site decoration, with an arrow marking a single ethene adsorbate; note the reduction in image adsorbate size on the saturated surface (image conditions: 30 Å × 30 Å, 77 K, 0.028 V, 0.131 nA).

(24) Kresse, G.; Hafner, J. *Phys. Rev. B* **1993**, *47*, 558−561.

(25) Kresse, G.; Furthmuller, J. *Comput. Mater. Sci.* **1996**, *6*, 15−50.
(26) Kresse, G.; Furthmuller, J. *Phys. Rev. B* **1996**, *54*, 11169−11186.

used for the calculations. This approach utilizes a plane-wave basis set, ultrasoft pseudopotentials,[27] and the generalized gradient approximation (GGA).[28,29] The GGA lattice constant for bulk silver is 2% larger than the experimental value (4.08 Å), yielding a Ag−Ag bond distance of 2.94 Å. The supercell approach is used to describe this complex surface, with each repeat unit containing three silver substrate layers and an O−Ag−O overlayer in a (4 × 4) unit cell. Along the {111} direction, the slabs are separated by a vacuum spacing of ∼15 Å. Gamma point calculations are performed here because of the large size of the unit cell.[30] The oxide trilayer and the top layer of the bare silver slab are fully relaxed. A molecule is then positioned on a variety of oxide binding sites, and a simultaneous relaxation of the adsorbate and the oxide trilayer is performed.

The STM image simulations employ a Green's function based elastic scattering formalism, described in detail elsewhere.[31,32] Significantly, this formalism allows a geometrical atom-by-atom description of the entire STM interface (surface and tip apex), providing a useful structural tool for direct comparison with the experimental tip structure. The same framework was recently used to simulate and explain the contrast found for STM images of the bare silver oxide surface.[2] For all the simulated images presented, the tip is modeled as an isolated rigid pyramid of W atoms stacked on top of a W{111} surface. No significant change in the calculated image contrast was observed from changing between a combination of tips (constructed from Pt or Ag atoms) or alternative terminating atoms such as oxygen. To determine the substrate geometry, we have used the VASP-derived, optimized structures, while the electronic structure has been approximated using an effective Hückel type Hamiltonian (EHT). The atomic orbital parameters involved in the EHT scheme have been determined from a least-squares fit to the density of states calculated by DFT.[33]

Theoretical Results

Models for the adsorption of a single ethene molecule on five different oxide sites are displayed in Figure 4. Adsorption upon all the symmetrically different silver sites (labeled Ag_n with $n = 1-5$ as indicated) was considered. In models a−d, the molecule sits above different silver atoms within the oxide layer. In model e, the molecule is positioned above an upper oxygen atom (O_u), located 0.7 Å above the silver layer.[4] We may define two types of silver that constitute the oxide overlayer: metallic silver (labeled Ag_1 and Ag_2) lying at the oxide ring center and electrophilic $Ag^{\delta+}$ silver (labeled Ag_3, Ag_4, and Ag_5) bonded to oxygen atoms in the oxide ring. Electronically equivalent atoms are grouped together; thus, Ag_1 and Ag_2 are discussed together as Ag_{1-2} (model a), and Ag_4 and Ag_5 are commonly termed as Ag_{4-5} (model d). The difference between Ag_3 and Ag_{4-5} originates from their respec-

(27) Vanderbilt, D. *Phys. Rev. B* **1990**, *41*, 7892−7895.
(28) Perdew, J. P.; Chevary, J. A.; Vosko, S. H.; Jackson, K. A.; Pederson, M. R.; Singh, D. J.; Fiolhais, C. *Phys. Rev. B* **1992**, *46*, 6671−6687.
(29) Perdew, J. P.; Chevary, J. A.; Vosko, S. H.; Jackson, K. A.; Pederson, M. R.; Singh, D. J.; Fiolhais, C. *Phys. Rev. B* **1993**, *48*, 4978−4978.
(30) This corresponds to 16 *k* points in the 1st Brillouin Zone of a (1 × 1) unit cell.
(31) Cerda, J.; Yoon, A.; Van Hove, M. A.; Sautet, P.; Salmeron, M.; Somorjai, G. A. *Phys. Rev. B* **1997**, *56*, 15900−15918.
(32) Cerda, J.; Van Hove, M. A.; Sautet, P.; Salmeron, M. *Phys. Rev. B* **1997**, *56*, 15885−15899.
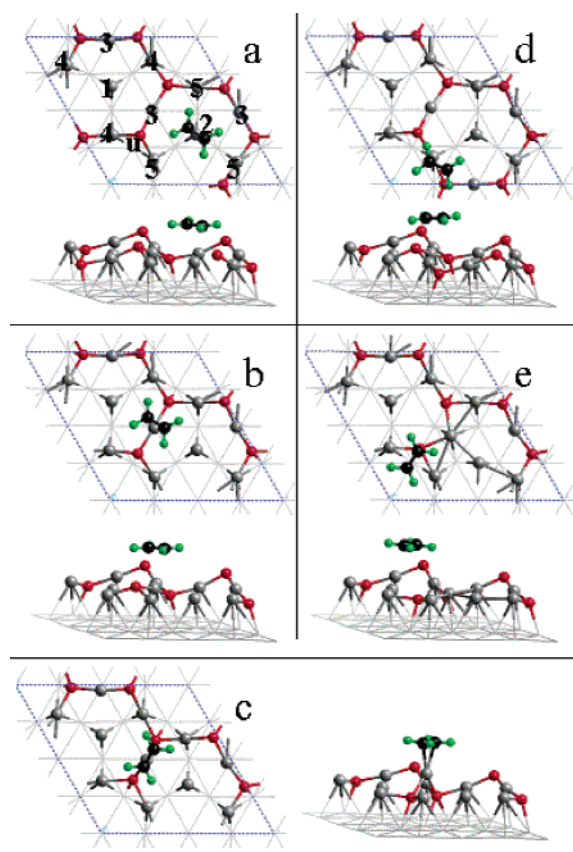(33) Cerda, J., Soria, F. *Phys. Rev. B* **2000**, *61*, 7965

Figure 4. Ball and stick representations of the five model unit cells of the catalyst−adsorbate system considered in this study. Specifically, a silver deficient oxide film on Ag{111}, with ethene adsorbed on five different labeled sites. Ag atoms in the oxide film are shown as light gray spheres and the Ag{111} substrate positions as light gray sticks. Red spheres represent the O atoms. For the adsorbate, spheres representing the carbon atoms are black, the green spheres indicate the position of hydrogen atoms. The oxygen atoms (red spheres) are further labeled with the letters u/d relating to their position in the upper/lower layer of the trilayer oxide structure.

tive coordination to the {111} substrate; Ag_3 is above an atop site, whereas the Ag_{4-5} site lies above threefold sites. Intuition would suggest that the ethene would adsorb on the lowest coordinated Ag_3 site, the highest atom in {111} direction. For this site, we have determined two stable orientations for the ethene molecular axis defined with respect to the perimeter of the oxide O−Ag−O rings. Model c shows the C−C bond parallel to this perimeter whereas model b places the C−C bond perpendicular to this direction. Different rotational configurations have also been tried for models a and b. Only a very small energy difference (1 kcal/mol) was seen between the rotational isomers indicating that the ethene orientation has a negligible effect for these weakly adsorbed sites.

Adsorption energies and structural results are reported in Table 1. Both the adsorption energy (E_b) and interaction energy (E_{int}) are given for each adsorption model. Upon adsorption, the surface distorts; E_{int} represents the strength of the bonding between ethene and the substrate already in its deformed geometry. Hence, the difference between the E_b and E_{int} is the energy required for the substrate deformation (E_{def}). Starting with the strongest binding site, the adsorption energy for the considered models decreases in the following order: c > a > b > d > e. In fact, models d and e are really nonbonding

Table 1. Structural Data Extracted from DFT Calculations Together with Relative Energies for the Models a–e As Shown in Figure 4[a]

model: site	a: Ag_{1-2}	b: $Ag_3 \perp$	c: Ag_3 //	d: Ag_{4-5}	e: O_u
d_{C-Ag} (Å)	2.7	2.9	2.3	3.2	3.8
d_{C-C} (Å)	1.34	1.34	1.37	1.33	1.33
$t_{C-C-H}(°)$	5	0	12	2	0
E_b(kJ/mol)	30	7	38	7	7
E_{int}(kJ/mol)	33	13	86	7	3
E_{def} (kJ/mol) $= E_{int} - E_b$	3	6	48	0	−4

[a] The adsorption energy (E_b) and interaction energy (E_{int}) are given for all computed sites. The two parameters have different zero-energy reference levels; for E_b, the reference levels are the energy of the gas-phase ethene molecule and the clean oxide surface in its equilibrium geometry; for E_{int}, the zero-energy point is the energy of the free ethene and the clean oxide surface distorted to the (artificial) geometry of the respective adsorbate system. The gas-phase C−C bond length is 1.33 Å for comparison with all models. The angle t(C−C−H) measures the hydrogen tilt relative to the molecular sp^2 C−C plane and thus quantifies the degree of sp^3 hybridization of the C atoms (originally sp^2, i.e., (t(C−C−H) = 0°). A pure sp^3 configuration would correspond to a maximum t(C−C−H) angle of 54.75°.

configurations, as their structural data show no molecular distortion in comparison with gas-phase ethene.

As suggested experimentally, model c is the most stable structure. This corresponds to adsorption above the Ag_3 site in one rigid configuration with the ethene C−C axis aligned to the side of the oxide hexagon, that is, parallel to the O−Ag_3−O bond (perpendicular to the perimeter of the honeycomb hexagons imaged). In this position, the C−C π^* orbitals overlap with the d orbitals of the Ag_3 atom. The quantitative values for model c, $E_b = 38$ kJ mol^{-1} and $E_{int} = 86$ kJ mol^{-1}, indicate moderate chemisorption associated with a slight sp^3 hybridization of ethene (~20% as measured in Table 1 by the t(C−C−H) angle). Surprisingly, the perpendicular axial orientation (site b), resulting from a 90° molecular rotation in the surface plane, is less stable by ~30 kJ mol^{-1}. Another moderately stable site appears to be Ag_{1-2} (model a). The C=C bond length is longer in model c, both in relation to that expected for the gas-phase molecule and also in comparison to all other sites. The increased bond length and the degree of sp^3 hybridization observed are significant and point to the activation of the adsorbed ethene molecule toward subsequent surface reactions such as epoxidation. The origin of Ag_3 as the preferred site, the influence of the C−C axial orientation, and the possibility of competitive adsorption on Ag_{1-2} all need to be qualitatively rationalized; these points are addressed in the discussion section.

The energy cost of the oxide deformation that accompanies adsorption may be considered by a comparison of the adsorption and interaction energies. Inspection of top and side views for models c and e (Figure 4) indicate that in these cases, molecular adsorption induces a substantial and visible deformation of the oxide registry. For model e, the lateral rearrangement of the surface results in the creation of a new Ag_3−Ag_1 bond by a local Ag_3 displacement and a simultaneous downward movement of the O target site. This distorted structure appears to correspond to a slight energy stabilization of the oxide surface, compared to the symmetric situation considered previously. However, this is an artifact of our restrictive k-mesh,[34] which offers no energetic dispersion for the symmetric (bare oxide) and asymmetric structures (the frozen configuration in model

(34) Both structures have been computed (static points only) with a denser k-grid (2 × 2 × 1) and the symmetric bare oxide is more stable than the asymmetric one by 0.25 eV.
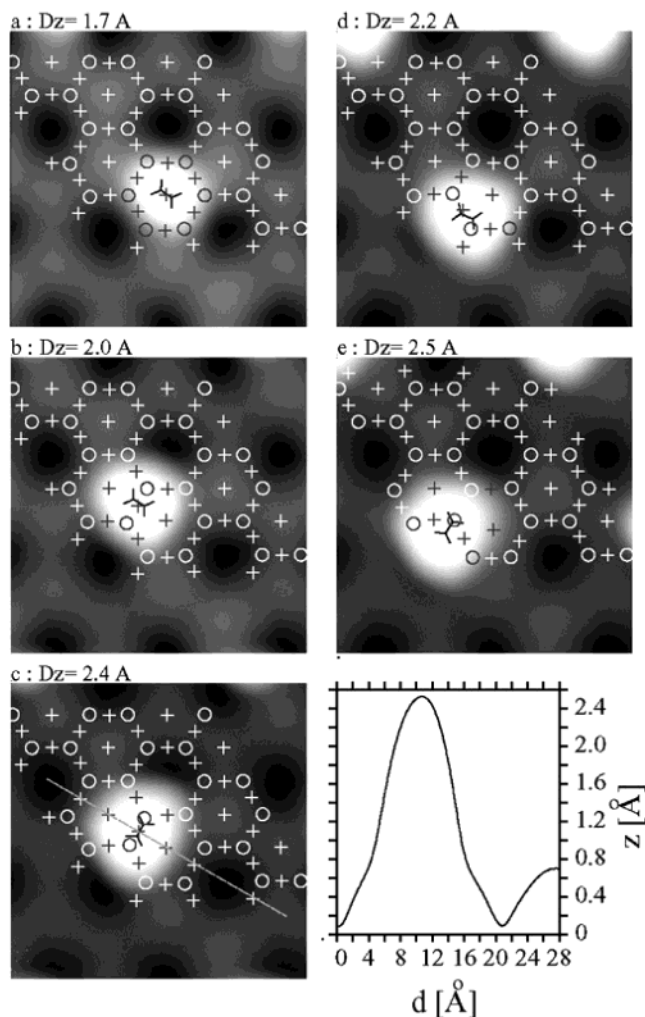

Figure 5. (a) STM simulations images of an (8 × 8) unit cell constructed from one (4 × 4) unit cell with adsorbed ethene and mapped with 3 units of the (4 × 4) clean oxide surface. This allows us to reduce the molecule coverage imposed by periodic DFT and facilitates comparison to Figure 1. The five images are 30 Å × 30 Å in size with $I = 1$ nA and $V = 50$ mV. Sticks mark the skeleton of the molecule (c and h), O and x, respectively, mark the registry of oxygen and silver atoms from the oxide film. These are computed in topographic mode yielding the marked corrugations. (b) A depth profile simulating the experimental line profile in Figure 1 is presented in the bottom right-hand corner.

e). Although this distortion demonstrates the flexibility of the oxide surface, ethene adsorption remains very weak in this position. This is not the case for model c, where a strong interaction energy between the molecule and the surface is achieved after oxide deformation. On the bare oxide, the Ag_3 atom is at intermediate height, located between an upward (O_u) and a downward (O_d) oxygen atom. Ethene adsorption completely reconstructs the surface; the Ag_3 atom is displaced outward, maximizing its interaction with the adsorbate. In a concerted action, the upward oxygen atom moves down toward the downward oxygen plane. The O−Ag−O angle, initially almost 180°, is strongly decreased to 89° after adsorption as pictured in Figure 7. In this way, the surface is strongly reconstructed, at a moderate energy cost, to optimize molecular adsorption.

In the second step, we simulate the topographic STM images (constant current mode) for the five optimized structures. Simulated images are shown in Figure 5a to associate the image

contrast to specific oxide sites. In all the images, ethene appears as the brightest protrusion, four times higher than the honeycomb feature characteristic of the oxide film. A qualitative comparison with Figure 1 allows the consideration of models b and c only; since the molecular feature is always centered between the honeycomb bumps and aligned between the honeycomb depressions. However, the simulations do not differentiate between the different orientations of ethene in model b and c. The agreement between simulated and experimental STM images is only qualitative, as demonstrated by comparing the extracted lines profiles in Figure 1 with Figure 5b. Although the honeycomb corrugation (2nd maximum) is 0.6 Å for model c (in excellent agreement with experiment), the maximum height of the adsorbed ethene in our simulation is 2.4 Å whereas it is ~1 Å experimentally. The contrast of the ethene molecule is hence overestimated in the simulation. Different tip apexes have been tested in the calculation with no significant change in the molecular topography. Following the recent argument of Rignanese et al.[35] applied for ethene adsorbed on $Si(001)-(2 \times 1)$ surface, the excess corrugation could be a DFT artifact, which intrinsically includes the self-interaction energy (SI). Using an accurate many-body formalism within a quasiparticle approach (called the GW approximation), the self-energy corrections for ethene states are about 1.5 eV larger than those for silicon states and thus induce a significant reduction of the ethene tunneling probability and protrusion height.

Discussion

Our DFT calculations demonstrate the following trend for preferential ethene adsorption on the oxide sites, in order of decreasing stability: $Ag_3 > Ag_{1-2} > Ag_{4-5}$. The main electronic difference between metallic Ag_{1-2} sites and electrophilic Ag_{4-5} and Ag_3 sites is located in their d-band density of states (DOS) shown in Figure 6, prior to ethene adsorption. The d contribution of the Ag_{1-2} atom produces a single peak, centered at −4 eV below the Fermi level, with no contribution above −3 eV. In contrast, the d-band of the Ag_3 and Ag_{4-5} atoms are composed of three contributions: a major peak, almost overlapping with that for Ag_{1-2} (around −3.7 eV), with two satellite peaks at lower energy (−6.5 eV, −5.5 eV) and two at higher energy (−2 eV, −1.5 eV). These satellite peaks are located exactly at the position of the oxygen p bands visible in Figure 6b and can be identified as the respective bonding and antibonding levels for the corresponding $O-Ag_3-O$ oxide linkages shown in Figure 6c. The differences between Ag_3 and Ag_{4-5} sites are subtler but remain visible after close comparison of the DOS in Figure 6a and 6b. First, there is a slight downshift of the d band center moving from Ag_3 to Ag_{4-5}; second, the antibonding states of $O-Ag_3-O$ (around −2 eV) have equal contribution from Ag, O_u (top oxygen layer), and O_d (bottom oxygen layer), but for $O-Ag_{4-5}-O$ the antibonding states are more developed (by a factor of 5/3) on the O_u and O_d. These two effects are closely related since a downshift of the center of the d-band for Ag_{4-5} may alter the interaction with the oxygen p orbitals by decreasing the metallic character of the antibonding states.

In ethene, we can restrict our orbital analysis to frontier π (located at −2.5 eV) and π^* (located around +3 eV) molecular orbitals. Upon adsorption, the main stabilizing interaction involves the vacant π^* orbital of ethene and the occupied d

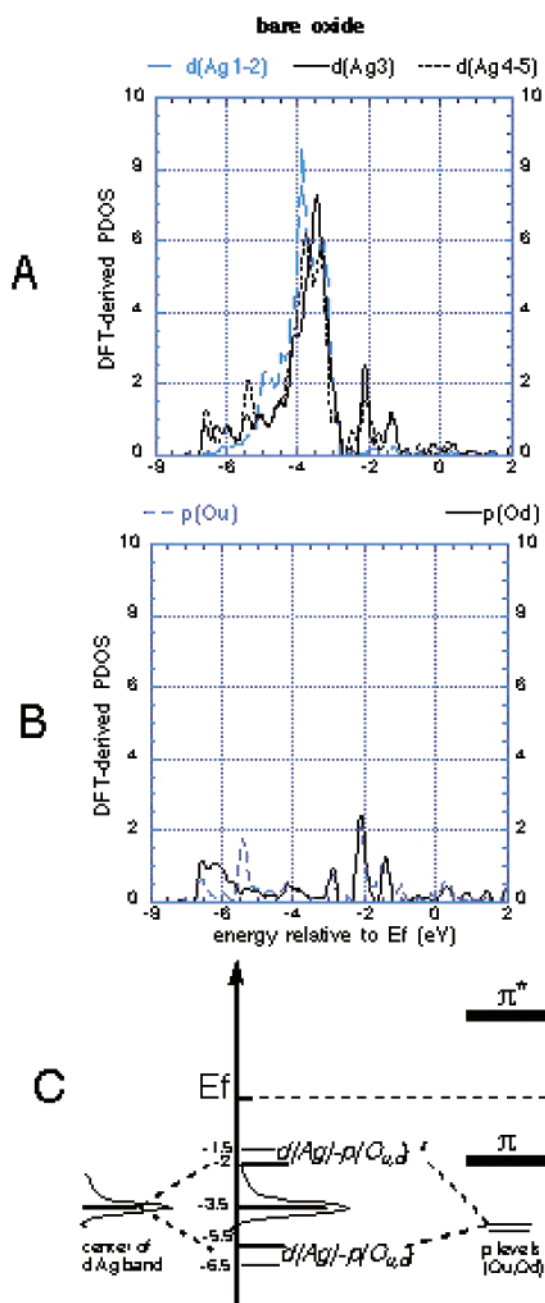(35) Rignanese, G. M.; Blase, X.; Louie, S. G. *Phys. Rev. Lett.* **2001**, *86*, 2110−2113.

Figure 6. Projected density of states derived from VASP calculations for the bare oxide: (A) d orbital projections for Ag sites (model a: Ag_{1-2}, models b and c: Ag_3, model d: Ag_{4-5}). s projections are of comparable energy but with intensities around 30 times smaller (omitted for clarity). (B) p orbital projections for the O_u and O_d oxygen species in the top and bottom layers, which neighbor the Ag sites (equivalent for sites Ag_3, Ag_4, and Ag_5). (C) Orbital interaction scheme to illustrate the above p DOS. Discrete levels on the right represent molecular orbital frontier levels for gas-phase ethene and atomic orbital p levels for oxygen prior to adsorption.

orbitals of the Ag site. For the electrophilic Ag_{4-5} and Ag_3 atoms, the antibonding $(O-Ag_3-O)^*$ states lie in the upper satellite bands, closer to the π^* orbital, resulting in a stronger molecule−surface interaction. This interaction is not favored on Ag_{1-2} since its d levels are low-lying in comparison to Ag_3 or Ag_{4-5}. The reduced d contribution to $(O-Ag_3-O)^*$ antibonding states observed on the Ag_{4-5} atom may explain the reduced reactivity of this site compared to Ag_3. However, geometric arguments could also play a role since Ag_{4-5} atoms
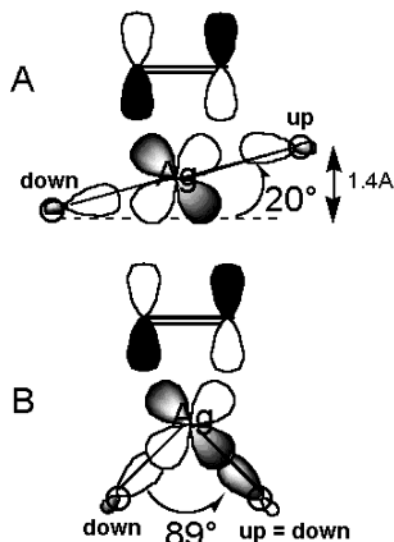
Figure 7. Schematic showing the orbital interaction between the π^* ethene orbital and the (O−Ag$_3$−O) reacting fragment: (A) for the clean oxide and (B) for the frozen oxide after parallel adsorption of ethene on Ag$_3$. The main deformation upon adsorption (case A to B) is a combined downward movement of one O$_u$ atom and a concerted upward movement by the Ag$_3$.

are less accessible than Ag$_{1-2}$ atoms, explaining the inversion of reactivity between Ag$_{4-5}$ and Ag$_{1-2}$, previously predicted by electronic considerations only.

The final question concerns the conformational selectivity; the parallel conformation with the C−C bond aligned along O−Ag−O ring edge is strongly preferred to the perpendicular C−C configuration. Again, as the simple scheme in Figure 7 shows, the key point is the main Ag d- C$_2$H$_4$ π^* interaction. In a perpendicular configuration, symmetry dictates that the π^* orbital can only overlap with the d orbitals perpendicular to O−Ag−O direction, that is, those which do not interact with the oxygen atoms and are located in the main d peak at low energy (−4 eV). In the parallel orientation, cooperative surface distortion allows the π^* orbital to interact with d states which can simultaneously overlap with oxygen orbitals. Hence, once the surface is distorted, the Ag$_3$ site offers both the highest energy d contribution and the best accessibility, both factors favoring molecular adsorption at this site. Compared to the metal, the Ag atom in the oxide film is activated, its d states being brought closer to the Fermi level by an antibonding combination with oxygen. However, this electronic activation alone is insufficient to explain the strong interaction with ethene; it is the relative flexibility of the oxide film that allows a deformation at relatively small cost in energy, which optimizes the overlap with the ethene molecular orbitals. Both electronic and steric arguments are required to account for the adsorption specificity.

Table 2. Associated Structural Data for Molecular Orientations A and B Drawn in Figure 7, Which Precisely Define the Deformation

distances in Å	Ag−O$_u$	Ag−O$_d$	Ag-{111}	O$_u$-{111}	O$_d$-{111}
bare oxide (prior to adsorption)	2.07	2.11	2.82	3.47	2.32
frozen oxide for model c	2.20	2.26	3.64	2.46	2.43

Conclusion

We have used low-temperature STM to image and characterize the adsorption of ethene on a complex reconstructed surface. Experimentally, one single adsorption site is suggested at both high and low exposure with the ethene on top of the electrophilic Ag$^{\delta+}$ atom in the oxide ring, which has the lowest coordination with respect to the underlying silver atoms. This is the Ag$_3$ site shown in Figure 2. Within a DFT framework, we have investigated a range of different possible sites to verify the experimental hypothesis. A thorough electronic and structural analysis of the possible configurations has enabled us to understand the site selectivity on this surface. Our calculations show that the experimental result corresponds to a unique orientation of ethene relative to the side of the hexagonal oxide ring. The energetic stability of adsorption at this site is an order of magnitude greater than simple adsorption on Ag{111} calculated using a similar method.[36] This may account for the activation of ethene when adsorbed on the catalytic oxide surface and demonstrates the key role of the oxygen atoms neighboring the active site.

The preferred configuration results from a local deformation of the catalyst structure which optimizes the interaction between the (O−Ag$_3$−O)* silver metallic states and the π^* levels of the ethene molecule. We have also simulated STM images associated with each configuration, which provide support for the experimental assignment of the favored site for ethene on the Ag$_3$ site. The simulations did not discriminate between parallel and perpendicular molecular orientations, for which DFT energetic calculations were required. This study clearly shows the power of combining STM experiments, DFT energetic calculations, and STM simulations to resolve and understand complex surface−adsorbate systems.

(36) We computed a binding energy of 6.3 kJ mol^{-1} for a Ag{111}-p(3 × 3)-C$_2$H$_4$ unit cell, in Bocquet, M.-L.; Rappe, A. M.; Dai, H. L., submitted to *Surf. Sci. Lett.*, 2003.